ARTICLE

doi:10.1038/nature09853

Crystal structure of inhibitor of κB kinase β

Guozhou Xu[1]*, Yu-Chih Lo[1]*, Qiubai Li[1], Gennaro Napolitano[2], Xuefeng Wu[2], Xuliang Jiang[3], Michel Dreano[4], Michael Karin[2] & Hao Wu[1]

Inhibitor of κB (IκB) kinase (IKK) phosphorylates IκB proteins, leading to their degradation and the liberation of nuclear factor κB for gene transcription. Here we report the crystal structure of IKKβ in complex with an inhibitor, at a resolution of 3.6 Å. The structure reveals a trimodular architecture comprising the kinase domain, a ubiquitin-like domain (ULD) and an elongated, α-helical scaffold/dimerization domain (SDD). Unexpectedly, the predicted leucine zipper and helix–loop–helix motifs do not form these structures but are part of the SDD. The ULD and SDD mediate a critical interaction with IκBα that restricts substrate specificity, and the ULD is also required for catalytic activity. The SDD mediates IKKβ dimerization, but dimerization per se is not important for maintaining IKKβ activity and instead is required for IKKβ activation. Other IKK family members, IKKα, TBK1 and IKK-i, may have a similar trimodular architecture and function.

Nuclear factor κB (NF-κB) transcription factors are master regulators of inflammatory, immune and apoptotic responses[1,2]. In the canonical pathway, NF-κB dimers are held in the cytoplasm through binding to IκB proteins, which mask their nuclear localization signals. When cells are stimulated by NF-κB inducers, IκB proteins are phosphorylated by the Ser/Thr-specific IKK, a modification that triggers their Lys-48-linked polyubiquitination and subsequent proteasomal degradation[3]. Freed NF-κB dimers enter the nucleus to regulate gene transcription[2]. In the non-canonical pathway, activated IKK phosphorylates the IκB-like domain in the NF-κB family member NF-κB2 (p49/p100)[3] (NFKB2 in humans). NF-κB signalling pathways are associated with a vast number of human diseases including inflammatory disorders and cancer, which renders IKK a potentially important therapeutic target[4] (see, for example, http://www.nf-kb.org).

IKK was originally purified from HeLa cells as a multiprotein complex that contains the kinase subunits IKKα (CHUK) and/or IKKβ (IKBKB), and the regulatory protein NEMO[5–11] (IKKγ, or IKBKG). IKKα and IKKβ both contain an amino-terminal kinase domain (KD), predicted leucine zipper (LZ) and helix–loop–helix (HLH) domains, and a carboxy-terminal NEMO-binding domain (Fig. 1a). IKKβ seems to have an additional ULD following the KD, which is not predicted in the corresponding region of IKKα[3]. The IKK-related kinases TBK1 (NAK) and IKK-i (IKK-ε, or IKBKE) seem to have a similar domain organization[12]. Whereas IKKβ mediates activation of the canonical NF-κB pathway in response to pro-inflammatory stimuli, IKKα has an indispensible role in non-canonical NF-κB signalling by phosphorylating NF-κB2 (p49/p100). Protein kinase assays suggest that IKKβ accounts for nearly all of the catalytic activity of the IKK holoenzyme towards IκBα[3,13] (NFKBIA).

The activation loop in both the IKKα and the IKKβ KD contains the mitogen-activated protein (MAP)-kinase kinase consensus motif SXXXS, where X is any amino acid[6–8,10] (Ser 177 and Ser 181 in human IKKβ). Some MAP-kinase kinase kinase family members, such as TGF-β-activated kinase 1 (MAP3K7, previously TAK1) and NF-κB-inducing kinase (MAP3K14, or NIK), were shown to phosphorylate IKKs[3,14,15]. IKKα and IKKβ can also undergo autophosphorylation and activation as a result of overexpression or signal-dependent NEMO clustering[10,16]. Ala substitutions of the activation-loop Ser residues prevent IKK activation whereas the phosphomimetic, double Glu mutation S177E/S181E (EE) of IKKβ renders it constitutively active[7,13].

Trimodular arrangement of IKKβ

We determined the crystal structure of *Xenopus laevis* IKKβ (ikbkb) EE (residues 4–675; Fig. 1a) in complex with either inhibitor Cmpd1 or inhibitor Cmpd2 (Supplementary Fig. 1) at resolutions of 4.0 and 3.6 Å in the $I4_122$ and $P1$ space groups, respectively (Supplementary Tables 1 and 2 and Supplementary Fig. 2). Eight IKKβ molecules in $P1$ and the single molecule in $I4_122$ are highly similar to each other (Supplementary Fig. 3 and Supplementary Table 3) and show conserved dimerization (see below). Our structural description will use the first dimer (chains A and B) in $P1$. The sequences of human and *Xenopus* IKKβ (henceforth hIKKβ and xIKKβ, respectively) have 74% identity with no gaps within the region of the structure; residue numbers designated for xIKKβ are also true for hIKKβ.

The IKKβ dimer structure resembles a pair of shears and has the overall dimensions of approximately 100 Å × 130 Å × 60 Å (Fig. 1b, c). It contains the KD (residues 16–307), the ULD (310–394) and the SDD (410–666) (Fig. 1a and Supplementary Fig. 4). The KD and the ULD form the 'handle' of the shears, and the SDD is the 'blade'. Both the KD and the ULD intimately associate with the SDD, suggesting that the KD does not function independently. Instead, the structure indicates that IKKβ is an integral trimodular unit.

The IKKβ KD in complex with either Cmpd1 or Cmpd2 has the typical bilobal kinase fold[17]. Although it has only 21.1% sequence identity with human ubiquitin, the ULD of IKKβ indeed has the ubiquitin fold (Fig. 1d). A major difference is the presence of an eight-residue insertion (373–380) that forms part of the loop connecting β-strands β4′ and β5′ in the ULD, which is mostly disordered. The hydrophobic surface patch of ubiquitin[18], which is often recognized by ubiquitin-binding proteins, is conserved in the ULD, with residues Val 318, Leu 354 and Leu 389 equivalent to Leu 8, Ile 44 and Val 70 of ubiquitin (Supplementary Fig. 5).

The SDD comprises six α-helices (α1s–α6s), of which α2s and α6s contain 70 and 77 residues, respectively. They twist together with a stretch of three shorter helices between them to fold as an elongated structural ensemble. The C lobe of the KD sits on the N-terminal end

[1]Department of Biochemistry, Weill Cornell Medical College, New York, New York 10021, USA. [2]Department of Pharmacology, University of California at San Diego, La Jolla, California 92093, USA. [3]EMD Serono Research Institute, Billerica, Massachusetts 01821, USA. [4]Merck Serono, Geneva 1211, Switzerland.
*These authors contributed equally to this work.

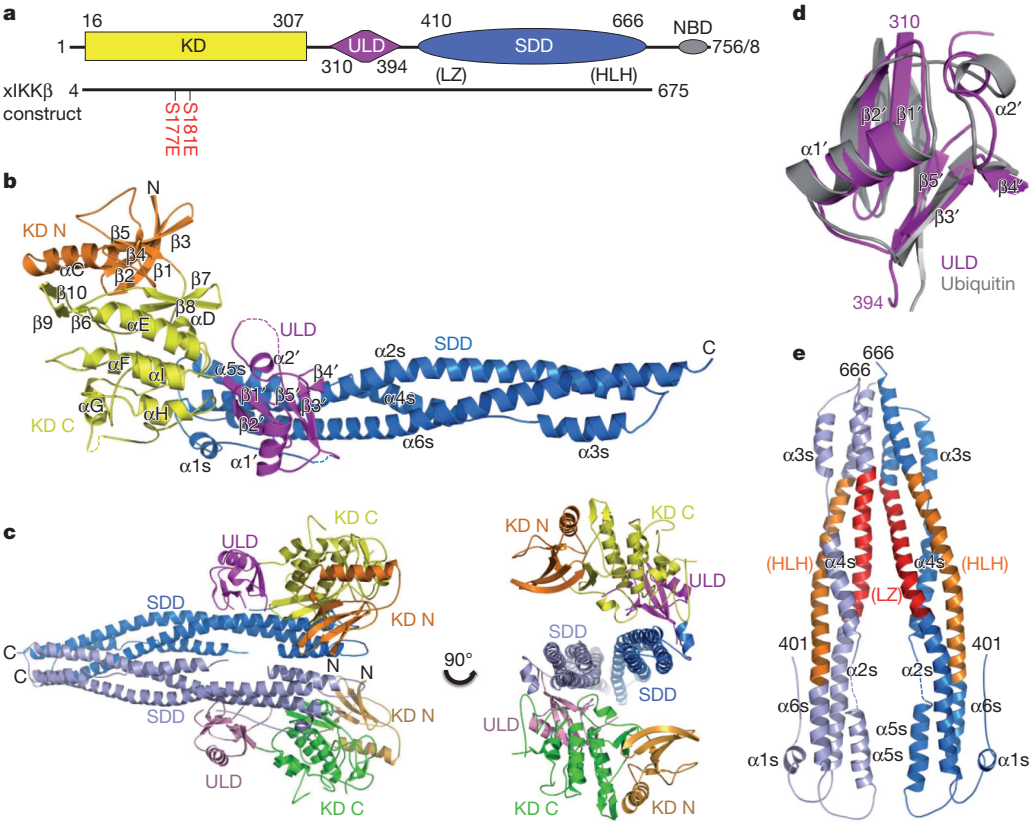

Figure 1 | Structure of xIKKβ. **a**, Linear representation of IKKβ showing the boundaries for the KD, the ULD and the SDD. Sequences of hIKKβ and xIKKβ are of 756 and 758 residues, respectively, and differ only at the most C-terminal region. The crystallized xIKKβ construct is shown. The previously designated LZ and HLH regions are shown in parentheses. **b**, Ribbon diagram of an xIKKβ protomer in the *P*1 crystal form. The N and C termini, KD N lobe (orange) and C lobe (yellow), ULD (magenta) and SDD (blue) are labelled. Secondary structural elements are labelled, with those in the ULD indicated with a prime and those in the SDD indicated with an 's'. **c**, Ribbon diagram of an xIKKβ dimer. **d**, Superposition of the ULD (magenta) with ubiquitin (grey). **e**, Ribbon diagram of an SDD dimer, showing locations of the previously designated LZ (red) and HLH (orange) regions.

of the SDD, and the ULD binds close to the middle of the SDD. Unexpectedly, formerly designated LZ (458–485) and HLH domains[7,8,10] (605–644) do not exist as such in the structure and are both part of the SDD (Fig. 1e). Most of the hydrophobic residues in the predicted LZ point inwards and are not available for mediating dimerization as previously proposed.

Structure of inhibitor-bound IKKβ KD

The inhibitor binds to the IKKβ KD at the hinge loop connecting the N and C lobes, a region that recognizes the adenine in ATP[19,20] and is often used for inhibitor binding[21–23] (Fig. 2a and Supplementary Fig. 6). The KD conformation is incompatible with that of an active kinase[17,24,25] (Fig. 2b, c). The activation segment, which begins from Asp 166-Leu 167-Gly 168 as the conserved DFG triad and extends to Ala 190-Pro 191-Glu 192 in the conserved APE motif, is fully ordered, including phosphomimetic residues Glu 177 and Glu 181 (Fig. 2b). However, the C-terminal anchor of the activation segment, including the APE motif, is completely out of place, with the result that essential interactions with the catalytic centre are lost (Fig. 2c). The gross conformation of the N-terminal anchor of the activation segment is preserved, with β9 paired with the β6 strand that precedes the catalytic loop. Part of the activation loop (175–177) contains an additional β-strand (β10), which sits between the lobes to form a three-stranded β-sheet with β9 and β6. The αC helix is tilted up and outwards (Fig. 2c) to make room for β10, which also disrupts its productive interactions with the DFG motif in active kinase structures.

Interactions among the KD, ULD and SDD

The KD, ULD and SDD interact mutually, with the ULD–SDD interaction being the most extensive, followed by the KD–SDD and KD–ULD

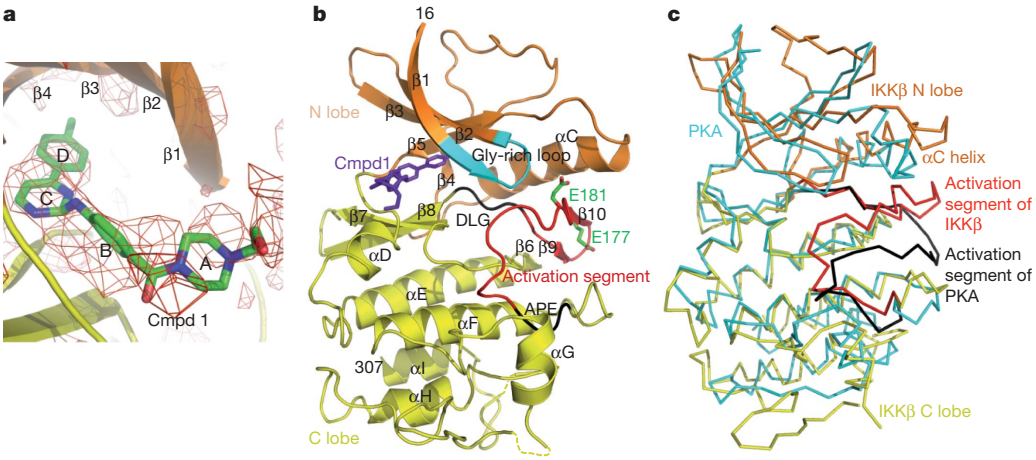

Figure 2 | Inhibitor-bound xIKKβ kinase domain. **a**, $F_o - F_c$ electron density map for Cmpd1 in the $I4_122$ structure, contoured at 2.0σ. Carbon, nitrogen and oxygen atoms are shown in green, blue and red, respectively. The four ring structures in Cmpd1 are labelled A, B, C and D, respectively. **b**, Structure of the xIKKβ KD. Gly-rich loop, cyan; activation segment, red (except that the DLG and APE sequences are in black); Cmpd1, purple. Side chains of phosphomimetic residues Glu 177 and Glu 181 are shown. **c**, Superposition of xIKKβ (orange and yellow) and protein kinase A (PKA, cyan; Protein Data Bank ID, 1ATP). The activation segments of xIKKβ and PKA are shown in red and black, respectively.

interactions. The ULD binds close to the middle of the SDD, contacting helices α2s and α6s (Fig. 3a). The interaction buries ~700 Å^2 of surface area per partner. There are substantial hydrophobic contributions, supplemented by electrostatic interactions. Residues Met 315, Met 317, Leu 354, Ile 387, Leu 389 and Phe 390 on one side of the ULD pack against Leu 612, Tyr 609, Leu 447 and the main chain of α2s of the SDD to form the central hydrophobic core of the interface. This hydrophobic patch of the ULD is immediately adjacent to and overlaps the conserved hydrophobic patch in the ubiquitin fold. Electrostatic interactions are observed between Glu 352 and Lys 619 and between Lys 394 and Asp 610. Additional interfacial residues include Ser 319 and Ser 357 of the ULD and Thr 453, Gln 449 and Val 616 of the SDD.

Consistent with an important role of the ULD in interacting with the SDD, mutations in residues that are not at the interface, P347A, L361A and Q351A, had minimal effects on NF-κB activation[26]. In contrast, mutation in a residue within a ULD surface loop that contacts the SDD, G358A (Fig. 3a), affected IKKβ-induced NF-κB activity[26]. It was also shown that Leu 353 is required for IKKβ activity[26]; however, Leu 353 is buried in the ULD core and the L353A mutation may have disrupted IKKβ structural integrity. Double substitutions of hIKKα and hIKKβ, which are equivalent to I608R/Y609P of the SDD of xIKKβ, did not affect their interaction with wild-type IKKβ but negatively impacted kinase activity[10]; Ile 608 is buried in the SDD core and Tyr 609 directly interacts with the ULD (Fig. 3a).

Like the ULD, the KD also makes contact with the N terminal end of the SDD (Fig. 3b), burying a surface area of ~650 Å^2 of each interface. The binding forces are mainly van der Waals in nature. Limited hydrophobic interactions are observed between residues Ala 252 and Val 253 of the KD and Tyr 423 of the SDD, and between Phe 111 of the KD and the hydrophobic portions of Arg 572, Arg 575 and Glu 576 of α5s of the SDD. The KD is linked to the ULD through a two-amino-acid linker between αI of the KD and β1′ of the ULD (Fig. 3c), burying only ~350 Å^2 of surface area. Side-chain contacts between Leu 311 of the ULD and Ile 268 of the KD are observed, and together form the small hydrophobic patch at the KD–ULD junction consisting also of Leu 269 and Ile 306 of the KD and Leu 309 of the linker. Together with the ionic interaction between Asp 373 of the ULD and Arg 123 of αE of the KD, these interactions may confer rigidity to the KD–ULD junction despite the small buried surface area.

Structural comparison with other kinase structures revealed a similarity between the locations of the SDD and ULD and those of several known docking sites for substrates and regulatory proteins[27]. In the crystal structure of the Ser/Thr kinase SRPK1 in complex with a docking motif in its substrate, ASF/SF2[27] (SRSF1), the peptide motif interacts with the kinase at the location of the SDD (Fig. 3d). In the structure of the TAK1 KD fused with the C-terminal region of its binding protein, TAB1[28], TAB1 interacts with the C lobe of the kinase at a position analogous to both the SDD and the ULD, presumably to activate the kinase (Fig. 3d).

ULD–SDD binds the IκBα C-terminal region

Previous studies have suggested that the ULD in TBK1 and IKK-i is involved in substrate recognition because its deletion impaired activity of the respective kinases and a glutathione *S*-transferase (GST)–ULD fusion protein interacted with the specific substrate, IRF3 or IRF7[29]. Because ULD deletion in IKKβ also abolished its activity[26], we proposed that the ULD may recognize its specific substrate, IκBα. However, we were surprised to find that GST–IκBα (1–317 and 54–317) pulled down only a minute amount of the ULD (Fig. 4a, lanes 9 and 13) and GST alone did not pull down any (Fig. 4a, lane 4), suggesting that the interaction of IκBα with the ULD is specific, but very weak. In contrast, GST–IκBα robustly pulled down full-length IKKβ or IKKβ lacking C-terminal NEMO-binding domain (Fig. 4a, lanes 15 and 16).

IκBα has an N-terminal region (1–54) that contains cognate phosphoacceptor sites at Ser 32 and S 36, followed by a C-terminal region (55–317) that contains multiple ankyrin repeats and the PEST region[30,31]. Strikingly, the N-terminal region of IκBα did not pull down any IKKβ constructs (Fig. 4a, lanes 5–8), and the C-terminal region of IκBα interacted robustly with full-length IKKβ as well as its ULD–SDD region (Fig. 4a, lanes 9–12), and very weakly with the ULD alone (Fig. 4a, lane 9). Further mapping on IκBα showed that both

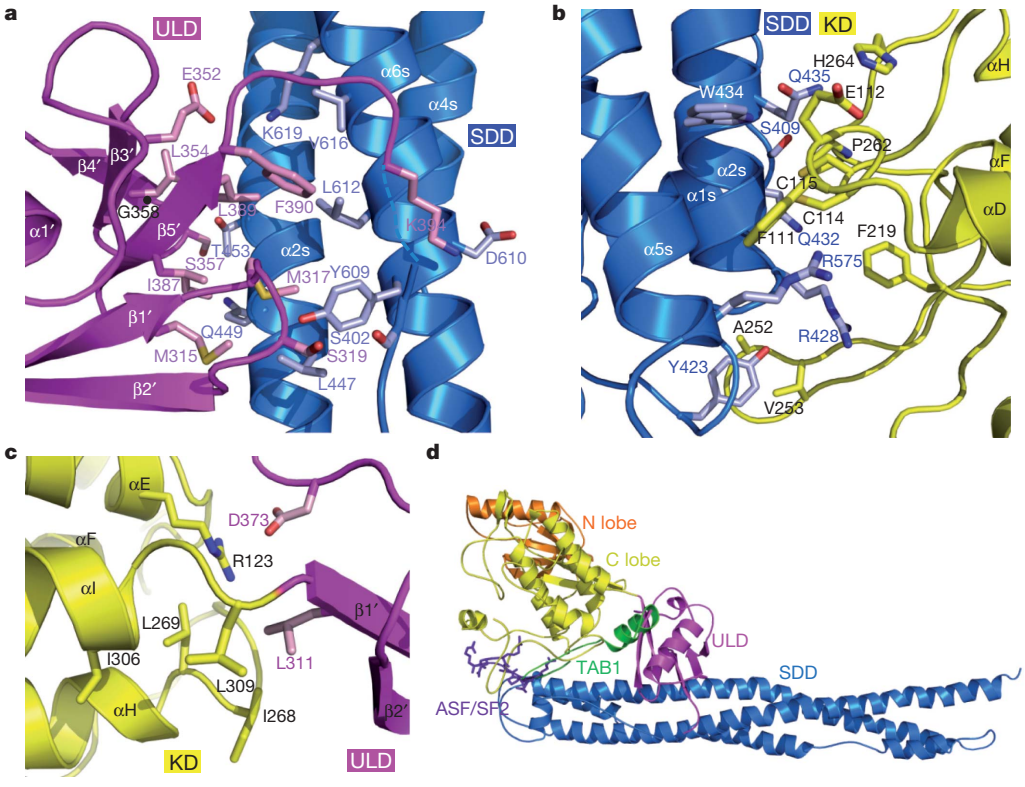

Figure 3 | Interactions among the KD, ULD and SDD. a, Interaction between the ULD (magenta) and SDD (blue). Important interfacial side chains are shown with nitrogen atoms in blue, oxygen atoms in red, sulphur atoms in orange and carbon atoms in either pink (ULD) or light blue (SDD). Gly 358 is marked with a black ball on the main chain. **b**, Interaction between the KD (yellow) and SDD (blue). **c**, Interaction between the KD (yellow) and ULD (magenta). **d**, Locations of the TAB1 peptide (green ribbon; PDB ID, 2EVA) and the ASF/SF2 peptide (purple stick model; PDB ID, 1WBP) relative to the IKKβ structure after superposition of the corresponding kinase domains.

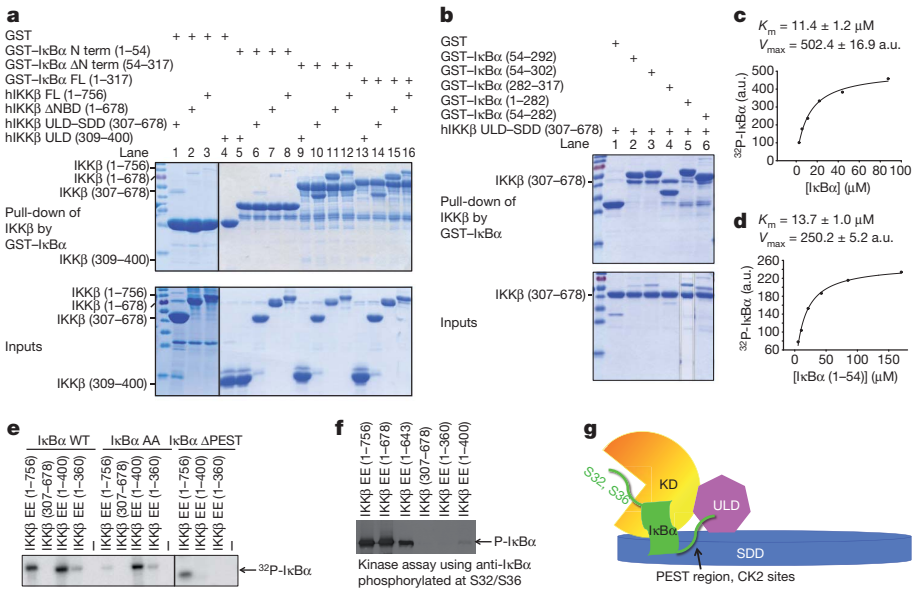

Figure 4 | ULD–SDD restricts IKKβ specificity and ULD is required for catalytic activity. **a**, **b**, Pull-down of hIKKβ constructs using GST–IκBα constructs, showing the reciprocal interaction between ULD–SDD of IKKβ and the C-terminal region of IκBα containing ankyrin repeats and the PEST region. FL, full length. **c**, **d**, Measurement of K_m and the relative V_{max} of IKKβ against full-length IκBα (**c**) and the N-terminal region of IκBα (1–54) (**d**). a.u., arbitrary units. **e**, Kinase assay of purified hIKKβ proteins against IκBα, its S32A/S36A mutant (AA) and its PEST-deletion construct (ΔPEST, 1–282) using [γ-^{32}P]ATP. WT, wild type. **f**, Kinase assay of purified hIKKβ proteins using antibody against IκBα phosphorylated at Ser 32 and Ser 36. **g**, Interaction between the SDD of IKKβ and the C-terminal region of IκBα may position the N-terminal cognate phosphorylation sites of IκBα at the active site of IKKβ. CK2, casein kinase 2.

ankyrin repeats (1–282 or 54–282) and the PEST region (282–317) interacted with IKKβ ULD–SDD (Fig. 4b, lanes 4–6). The extent of pull-down suggests that the PEST region contributes more to IKKβ interaction than do the ankyrin repeats. Despite trying multiple constructs, we could not obtain soluble protein for IKKβ SDD to test its interaction with IκBα. However, the pull-down data suggest a dominant role for SDD in IκBα interaction. In any case, it is clear that the mutual interaction between IKKβ and IκBα is mediated by their ULD–SDD and C-terminal domains, respectively.

ULD–SDD limits specificity and the ULD aids catalysis

The specific interaction between ULD–SDD of IKKβ and IκBα suggests that the Michaelis constant, K_m, of phosphorylation by IKKβ might be lower for full-length IκBα than for its N-terminal region (1–54) alone. We performed kinase kinetics analysis of IKKβ EE against the two different substrates. Unexpectedly, the measured apparent K_m values were 11.4 and 13.7 μM for full-length IκBα and the N-terminal region alone, respectively (Fig. 4c, d), suggesting that binding at the SDD, an exosite, does not alter the K_m of the reaction drastically. This could be due to opposing effects of the SDD–IκBα interaction, which increases substrate interaction but slows down product dissociation. The relative maximum velocity, V_{max}, values were 502.4 and 250.2, respectively, suggesting that the SDD–IκBα interaction moderately enhances catalysis.

Casein kinase 2 phosphorylates the C-terminal PEST region of IκBα around residues 283–299[30,31]. To determine whether the SDD–IκBα interaction restricts substrate specificity, we compared the kinase activity of purified IKKβ EE proteins against either IκBα or its S32A/S36A mutant (AA) using [γ-^{32}P]ATP (Fig. 4e). Although the KD–ULD (1–400) construct gave rise to a small amount of protein, it produced robust phosphorylation of wild-type IκBα, comparable to full-length IKKβ (1–756), suggesting that it is catalytically competent. Remarkably, KD–ULD effectively phosphorylated the AA mutant, which, in contrast, was a poor substrate for full-length IKKβ. The C-terminal PEST region seemed to harbour the major sites of phosphorylation by KD–ULD because a construct lacking PEST (1–282) was not significantly phosphorylated by KD–ULD but was phosphorylated by full-length IKKβ (Fig. 4e). In addition, when IκBα phosphorylation was detected by antibody against IκBα phosphorylated at Ser 32/Ser 36, only very weak phosphorylation was seen for the KD–ULD construct in comparison with full-length IKKβ (Fig. 4f). These experiments suggest that although the KD–ULD construct is active, it possesses an altered substrate specificity causing preferential phosphorylation of the C-terminal PEST sequence, consistent with a previous observation[32]. Hence, ULD–SDD seems to position IκBα specifically such that only its N-terminal region is accessible to the IKKβ catalytic pocket (Fig. 4g).

We expressed three kinase domain constructs, 1–301, 1–310 and 1–360, in insect cells and obtained only small amount of protein for the 1–360 construct. Kinase assay showed that IKKβ EE (1–360) had very low residual activity against IκBα or its AA mutant (Fig. 4e), suggesting that KD activity is compromised in the absence of the ULD. Without an isolated KD structure, we cannot deduce the molecular mechanism by which the ULD acts. However, in analogy to TAK1 activation by TAB1[28] (Fig. 3d), it may be speculated that this KD–ULD interaction allosterically potentiates kinase activity. Further kinase assay using antibody against IκBα phosphorylated at Ser 32/Ser 36 showed no detectable activity of the KD alone (Fig. 4f), confirming that the low residual activity may also be directed towards the C-terminal PEST region, similar to KD–ULD. Therefore, whereas ULD–SDD is critical for IKKβ specificity, ULD is required for its catalytic activity.

SDD mediates IKKβ dimerization

Full-length hIKKβ (1–756) and its KD–ULD–SDD region (1–678) are dimers in solution as determined by gel-filtration chromatography (Fig. 5a). In the *P*1 and $I4_122$ crystals, two conserved dimerization interfaces exist, one mediated by the SDD and the other mediated by the KD. Because hIKKβ (1–643) that truncates into the SDD is a monomer in solution (Fig. 5a), SDD-mediated dimerization (Fig. 5b) is probably of greater importance than KD-mediated dimerization.

SDD in an IKKβ dimer does not form extensive interactions along the entire length dimension of the helical bundle. Rather, interactions are mostly localized at the end of the bundle (Fig. 5b), distal from the KD and ULD and burying ~1,000 Å^2 of surface area of each monomer. The interaction is mostly hydrophobic. Residues that contribute significantly to dimerization include Gln 478, Lys 482, Phe 485, Ile 492, Lys 496, Ile 505, Gln 651, Leu 654, Trp 655, Leu 658 and Ile 660, with residues Leu 654, Trp 655 and Leu 658 from helix α6s burying the most surface area (Fig. 5b). This dimerization interface is entirely unexpected as it was predicted earlier that the LZ mediates IKKβ dimerization. The structure now explains that failed dimerization of the LZ-defective L462S/L469S mutant of IKKα[10] is due to the structural role of Leu 469, whose equivalent residue of IKKβ, Met 472, is buried in the SDD core. Superposition of four IKKβ dimers in *P*1

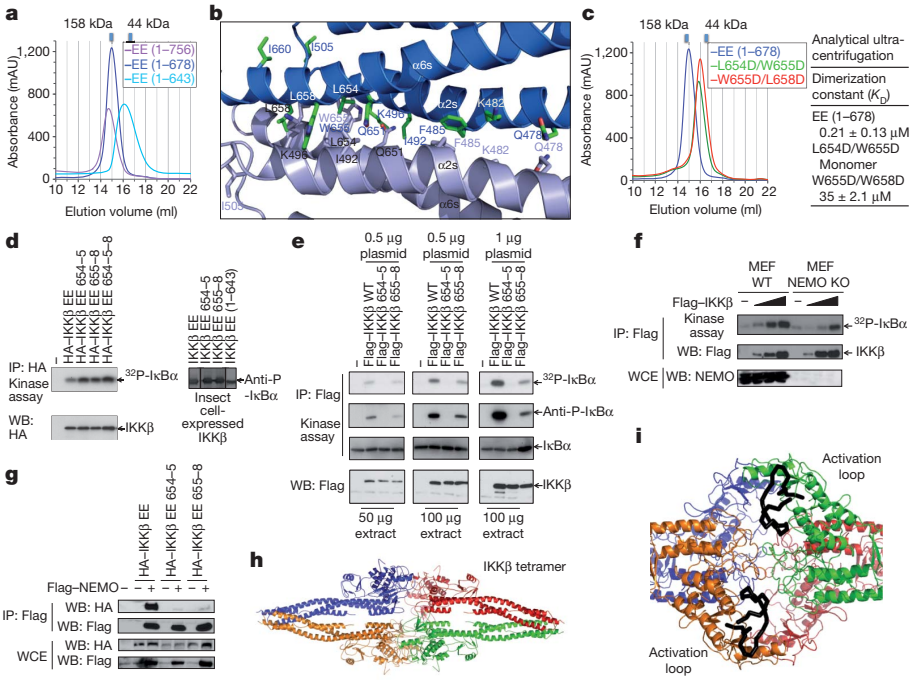

Figure 5 | Dimerization is critical for IKKβ activation but not for its activity. **a**, Gel filtration profiles of various hIKKβ constructs showing that those containing the KD–ULD–SDD region (1–756, 1–678) are dimeric and that a further truncated construct (1–643) is monomeric. mAU, milliabsorbance unit. **b**, The dimerization interface of xIKKβ. **c**, Structure-based mutations disrupt hIKKβ dimerization as shown by gel filtration and analytical ultracentrifugation. **d**, Kinase activity of HEK293T-cell-transfected or insect-cell-purified hIKKβ EE and dimerization-defective mutants L654D/W655D (654–655), W655D/L658D (655–658) and L654D/W655D/L658D (654–655–658). **e**, Autoactivation of HEK293T-cell-transfected wild-type hIKKβ and its dimerization-defective mutants. **f**, Transfection of hIKKβ into wild-type and NEMO$^{-/-}$ mouse embryonic fibroblasts (MEFs), showing reduced IKKβ activation in the absence of NEMO. **g**, Dimerization mutants of IKKβ showing reduced interaction with NEMO. **h**, Tetramer of xIKKβ in the *P*1 structure. **i**, Close-up view of the tetramer interface, showing that the activation loops of neighbouring protomers (black) face each other.

and the single IKKβ dimer in $I4_122$ shows that IKKβ dimers are conserved (Supplementary Fig. 7). In $I4_122$, the distal part of the SDD is not visible, owing to a lack of crystal packing in this region and dynamic disorder, not degradation (Supplementary Fig. 8).

To confirm the observed interface in IKKβ dimerization, we performed structure-based mutagenesis on residues that bury the most surface area, Leu 654, Trp 655 and Leu 658. These residues are not within the predicted LZ region. Two purified double mutants, L654D/W655D and W655D/L658D, failed to dimerize, as shown by the considerable shift in gel filtration positions (Fig. 5c). Furthermore, equilibrium analytical ultracentrifugation experiments showed that wild-type IKKβ is indeed a dimer whereas one of the IKKβ mutants is a monomer and the other has a 167-fold weaker dimerization affinity (Fig. 5c).

Dimerization in IKKβ activation but not activity

The geometry of the IKKβ dimer with KDs facing away from each other suggests that each IKKβ protomer is independent in its kinase activity. To confirm this, we transfected HEK293T cells with hIKKβ EE mutants, L654D/W655D (654–655), W655D/L658D (655–658) and L654D/W655D/L658D (654–655–658), and found that all mutants had robust kinase activity (Fig. 5d). Dimerization mutants expressed in insect cell and purified showed the same results. In addition, a purified IKKβ construct with truncation into the SDD (1–643) that is monomeric in solution (Fig. 5a) was active in phosphorylating IκBα (Fig. 5d).

Previous studies have shown that IKKβ can undergo *trans*-autophosphorylation and activation on transfection[13,16]. This autophosphorylation and phosphorylation by TAK1 probably both contribute to IKKβ activation on cell stimulation. To determine whether the observed dimerization interface is critical for this activation, we tested dimerization mutations in IKKβ activation on overexpression in HEK293T cells (Fig. 5e). Whereas wild-type IKKβ was robustly activated, the L654D/W655D and W655D/L658D mutants completely and partly lost this activation, respectively, in a manner that correlates with the degree of impairment in dimerization (Fig. 5c, e). Overexpression of IKKβ in NEMO-deficient mouse embryonic fibroblasts resulted in its activation, but to a lesser extent than in wild-type mouse embryonic fibroblasts (Fig. 5f). We found that IKKβ dimerization mutants failed to interact with NEMO efficiently (Fig. 5g), perhaps owing to reduced avidity for oligomeric NEMO. Therefore, although IKKβ kinase activity does not depend on dimerization once its activation loop is phosphorylated, IKKβ activation requires dimerization and is probably enhanced by interaction with NEMO.

Discussion

The IKKβ structure presented here predicts that IKKα, TBK1 and IKK-i all have an overall structural organization that comprises KD, ULD and SDD. Although a ULD was not predicted in IKKα, conservation of buried residues in this region and of the ULD–SDD interface suggests that IKKα also has this domain (Supplementary Fig. 4). The ULD and SDD probably have the same structural role but may have evolved additional, differential functions in the individual kinases. SDD-mediated dimerization may also be conserved. In particular, residues at the observed IKKβ dimerization interface are highly conserved in IKKα (Supplementary Fig. 4), explaining how IKKα and IKKβ can form both homo- and heterodimers[8,13]. Given our structure of IKKβ and the previously determined structures of NEMO fragments[33–37], we may speculate that the full IKK complex is also a dimer, or a dimer of dimers with a molecular mass of around 270 or 540 kD. The apparent 700–900-kD molecular mass of the IKK holoenzyme on gel filtration[5–10] may be due to the elongated nature of NEMO and the complex (Supplementary Fig. 9).

Because the conserved IKKβ dimer structure does not place the KDs close to each other for *trans*-autophosphorylation, we wondered whether higher-order oligomerization, which is probably enhanced by NEMO and its ability to bind ubiquitin[33,34], is responsible for this autoactivation. In both *P*1 and $I4_122$, IKKβ exists as dimers of dimers (Fig. 5h and Supplementary Fig. 10). In particular, active sites of two neighbouring protomers in the tetramer face each other such that an activation loop from one protomer might reach into the active site of the other (Fig. 5i), which may mimic an autophosphorylation state.

The ULD–SDD region of IKKβ directly interacts with the C-terminal portion of IκBα. This interaction may serve several purposes. First, it probably orients IκBα such that its N-terminal cognate phosphorylation sites are presented to the KD active site (Fig. 4g). Without this interaction, IKKβ preferentially phosphorylates the C-terminal PEST motif of IκBα. Second, the interaction seems to enhance IKKβ activity. Third, phosphorylation at the PEST by casein kinase 2 or other kinases may regulate IκBα interaction with IKKβ

and hence affect phosphorylation at the cognate sites. Fourth, the interaction may allow concerted phosphorylation at both Ser 32 and Ser 36 of IκBα without intervening dissociation. In MAP-kinase cascades that involve dual phosphorylations, specific docking interactions occur between the kinases and their substrates[27,38,39]. The β-catenin protein in the Wnt signalling pathway contains the same dual-phosphorylated destruction box motif as IκBα (ref. 40). Consistent with this, β-catenin is brought to the responsible kinase, GSK-3, by means of the adaptor protein axin, allowing both specificity and concerted phosphorylation[41,42]. Therefore, in a general statement that structure serves function, the IKKβ structure seems to fit its function as the IκBα kinase perfectly, being poised to turn on the important NF-κB pathway specifically, efficiently and concertedly in response to cellular physiology.

METHODS SUMMARY

Xenopus laevis IKKβ was expressed in insect cells and purified to homogeneity using nickel affinity chromatography, ion exchange and gel filtration chromatography. We crystallized the *P*1 and $I4_122$ forms at 4 °C in polyethylene glycol 6000 and potassium/sodium phosphate, respectively. The structure was determined by multiwavelength anomalous diffraction of the selenomethionyl protein.

Full Methods and any associated references are available in the online version of the paper at www.nature.com/nature.

Received 27 September 2010; accepted 17 January 2011.
Published online 20 March 2011.

1. Hayden, M. S. & Ghosh, S. Shared principles in NF-κB signaling. *Cell* **132,** 344–362 (2008).
2. Vallabhapurapu, S. & Karin, M. Regulation and function of NF-κB transcription factors in the immune system. *Annu. Rev. Immunol.* **27,** 693–733 (2009).
3. Scheidereit, C. IκB kinase complexes: gateways to NF-κB activation and transcription. *Oncogene* **25,** 6685–6705 (2006).
4. Karin, M. Nuclear factor-κB in cancer development and progression. *Nature* **441,** 431–436 (2006).
5. Chen, Z. J., Parent, L. & Maniatis, T. Site-specific phosphorylation of IκBα by a novel ubiquitination-dependent protein kinase activity. *Cell* **84,** 853–862 (1996).
6. DiDonato, J. A. *et al.* A cytokine-responsive IκB kinase that activates the transcription factor NF-κB. *Nature* **388,** 548–554 (1997).
7. Mercurio, F. *et al.* IKK-1 and IKK-2: cytokine-activated IκB kinases essential for NF-κB activation. *Science* **278,** 860–866 (1997).
8. Woronicz, J. D. *et al.* IκB kinase-β: NF-κB activation and complex formation with IκB kinase-α and NIK. *Science* **278,** 866–870 (1997).
9. Yamaoka, S. *et al.* Complementation cloning of NEMO, a component of the IκB kinase complex essential for NF-κB activation. *Cell* **93,** 1231–1240 (1998).
10. Zandi, E. *et al.* The IκB kinase complex (IKK) contains two kinase subunits, IKKα and IKKβ, necessary for IκB phosphorylation and NF-κB activation. *Cell* **91,** 243–252 (1997).
11. Rothwarf, D. M., Zandi, E., Natoli, G. & Karin, M. IKK-γ is an essential regulatory subunit of the IκB kinase complex. *Nature* **395,** 297–300 (1998).
12. Hacker, H. & Karin, M. Regulation and function of IKK and IKK-related kinases. *Sci. STKE* **2006,** re13 (2006).
13. Zandi, E., Chen, Y. & Karin, M. Direct phosphorylation of IκB by IKKα and IKKβ: discrimination between free and NF-κB-bound substrate. *Science* **281,** 1360–1363 (1998).
14. Sato, S. *et al.* Essential function for the kinase TAK1 in innate and adaptive immune responses. *Nature Immunol.* **6,** 1087–1095 (2005).
15. Liu, H. H., Xie, M., Schneider, M. D. & Chen, Z. J. Essential role of TAK1 in thymocyte development and activation. *Proc. Natl Acad. Sci. USA* **103,** 11677–11682 (2006).
16. Tang, E. D. *et al.* Roles for homotypic interactions and transautophosphorylation in IκB kinase (IKKβ) activation. *J. Biol. Chem.* **278,** 38566–38570 (2003); erratum **278,** 49661 (2003).
17. Knighton, D. R. *et al.* Crystal structure of the catalytic subunit of cyclic adenosine monophosphate-dependent protein kinase. *Science* **253,** 407–414 (1991).
18. Dikic, I., Wakatsuki, S. & Walters, K. J. Ubiquitin-binding domains — from structures to functions. *Nature Rev. Mol. Cell Biol.* **10,** 659–671 (2009).
19. Zheng, J. *et al.* 2.2 Å refined crystal structure of the catalytic subunit of cAMP-dependent protein kinase complexed with MnATP and a peptide inhibitor. *Acta Crystallogr. D* **49,** 362–365 (1993).
20. Bossemeyer, D. *et al.* Phosphotransferase and substrate binding mechanism of the cAMP-dependent protein kinase catalytic subunit from porcine heart as deduced from the 2.0 Å structure of the complex with Mn^{2+} adenylyl imidodiphosphate and inhibitor peptide PKI(5–24). *EMBO J.* **12,** 849–859 (1993).
21. Xu, R. M., Carmel, G., Kuret, J. & Cheng, X. Structural basis for selectivity of the isoquinoline sulfonamide family of protein kinase inhibitors. *Proc. Natl Acad. Sci. USA* **93,** 6308–6313 (1996).
22. Sicheri, F., Moarefi, I. & Kuriyan, J. Crystal structure of the Src family tyrosine kinase Hck. *Nature* **385,** 602–609 (1997).
23. Noble, M. E., Endicott, J. A. & Johnson, L. N. Protein kinase inhibitors: insights into drug design from structure. *Science* **303,** 1800–1805 (2004).
24. Nolen, B., Taylor, S. & Ghosh, G. Regulation of protein kinases; controlling activity through activation segment conformation. *Mol. Cell* **15,** 661–675 (2004).
25. Jeffrey, P. D. *et al.* Mechanism of CDK activation revealed by the structure of a cyclinA-CDK2 complex. *Nature* **376,** 313–320 (1995).
26. May, M. J. *et al.* A novel ubiquitin-like domain in IκB kinase β is required for functional activity of the kinase. *J. Biol. Chem.* **279,** 45528–45539 (2004).
27. Goldsmith, E. J. *et al.* Substrate and docking interactions in serine/threonine protein kinases. *Chem. Rev.* **107,** 5065–5081 (2007).
28. Brown, K. *et al.* Structural basis for the interaction of TAK1 kinase with its activating protein TAB1. *J. Mol. Biol.* **354,** 1013–1020 (2005).
29. Ikeda, F. *et al.* Involvement of the ubiquitin-like domain of TBK1/IKK-i kinases in regulation of IFN-inducible genes. *EMBO J.* **26,** 3451–3462 (2007).
30. Kato, T. Jr, Delhase, M., Hoffmann, A. & Karin, M. CK2 is a C-terminal IκB kinase responsible for NF-κB activation during the UV response. *Mol. Cell* **12,** 829–839 (2003).
31. Barroga, C. F., Stevenson, J. K., Schwarz, E. M. & Verma, I. M. Constitutive phosphorylation of I kappa B alpha by casein kinase II. *Proc. Natl Acad. Sci. USA* **92,** 7637–7641 (1995).
32. Shaul, J. D., Farina, A. & Huxford, T. The human IKKβ subunit kinase domain displays CK2-like phosphorylation specificity. *Biochem. Biophys. Res. Commun.* **374,** 592–597 (2008).
33. Lo, Y. C. *et al.* Structural basis for recognition of diubiquitins by NEMO. *Mol. Cell* **33,** 602–615 (2009).
34. Rahighi, S. *et al.* Specific recognition of linear ubiquitin chains by NEMO is important for NF-κB activation. *Cell* **136,** 1098–1109 (2009).
35. Rushe, M. *et al.* Structure of a NEMO/IKK-associating domain reveals architecture of the interaction site. *Structure* **16,** 798–808 (2008).
36. Bagnéris, C. *et al.* Crystal structure of a vFlip-IKKγ complex: insights into viral activation of the IKK signalosome. *Mol. Cell* **30,** 620–631 (2008).
37. Cordier, F. *et al.* Solution structure of NEMO zinc finger and impact of an anhidrotic ectodermal dysplasia with immunodeficiency-related point mutation. *J. Mol. Biol.* **377,** 1419–1432 (2008).
38. Remenyi, A., Good, M. C. & Lim, W. A. Docking interactions in protein kinase and phosphatase networks. *Curr. Opin. Struct. Biol.* **16,** 676–685 (2006).
39. Kallunki, T., Deng, T., Hibi, M. & Karin, M. c-Jun can recruit JNK to phosphorylate dimerization partners via specific docking interactions. *Cell* **87,** 929–939 (1996).
40. Wu, G. *et al.* Structure of a β-TrCP1-Skp1-β-catenin complex: destruction motif binding and lysine specificity of the SCF(β-TrCP1) ubiquitin ligase. *Mol. Cell* **11,** 1445–1456 (2003).
41. Ikeda, S. *et al.* Axin, a negative regulator of the Wnt signaling pathway, forms a complex with GSK-3β and beta-catenin and promotes GSK-3β-dependent phosphorylation of β-catenin. *EMBO J.* **17,** 1371–1384 (1998).
42. Hart, M. J. *et al.* Downregulation of β-catenin by human Axin and its association with the APC tumor suppressor, β-catenin and GSK3β. *Curr. Biol.* **8,** 573–581 (1998).

Supplementary Information is linked to the online version of the paper at www.nature.com/nature.

Acknowledgements We thank K. Rajashankar and N. Sukumar for data collection at the NE-CAT of APS, B. Schwer for help with the kinase assay, P. Gaillard for help with the chemistry and G. Ahlsen, L. Shapiro and B. Honig for the ultracentrifugation experiments. This work was supported by the National Institutes of Health (H.W. and M.K.), the American Heart Association (G.X. and Y.-C.L.) and the Cancer Research Institute (Y.-C.L.). M.K. is an American Cancer Society Research Professor.

Author Contributions G.X. cloned, expressed, purified, crystallized and determined the crystal structure of xIKKβ and performed experiments to determine K_m. Y.-C.L. cloned, expressed, purified and crystallized hIKKβ and performed pull-down experiments and kinase assays using phospho-IκBα antibody. Q.L. expressed the hIKKβ mutants in insect cells. G.N. and X.W. performed transfection, immunoprecipitation and kinase assays and M.K. supervised these experiments. H.W. supervised the project. G.X and H.W. made the figures and wrote the manuscript.

Author Information Atomic coordinates and structure factors have been deposited in the Protein Data Bank under accession codes 3QA8 and 3QAD. Reprints and permissions information is available at www.nature.com/reprints. The authors declare no competing financial interests. Readers are welcome to comment on the online version of this article at www.nature.com/nature. Correspondence and requests for materials should be addressed to H.W. (haowu@med.cornell.edu).

METHODS

Protein expression and purification. To elucidate the molecular basis of IKKβ function, we expressed IKKβ from a number of species using baculovirus-mediated insect cell expression. The xIKKβ sequence in the NCBI database starts at a Met residue that is equivalent to Met 17 of both the hIKKβ and the mouse IKKβ (mIKKβ) sequence. Translation of the DNA sequence preceding the ATG codon of Met 17 revealed sequences that are almost identical to residues 9–16 of hIKKβ and mIKKβ. These were taken as part of the xIKKβ sequence and residues 1–8 were taken from the corresponding mIKKβ sequence. This reconstructed xIKKβ sequence has the same residue numbering as the hIKKβ sequence until after the SDD.

Various constructs of IKKβ wild type and the phosphomimetic S177E/S181E mutant were designed with an N-terminal polyhistidine tag and a tobacco etch virus protease-cutting site between the tag and the protein. Recombinant IKKβ baculoviruses were made in DH10BAC cells, amplified and used to infect Hi5 insect cells in serum-free media (Invitrogen). The cells were cultured in suspension and harvested 48 h after infection. The recombinant proteins were purified by nickel affinity chromatography, anion exchange and gel filtration chromatography. For crystallization, the polyhistidine tag was cleaved by the tobacco etch virus protease during protein purification.

All IκBα proteins were expressed in *Escherichia coli* using pET28a, pGEX4T3 and pET-SUMO vectors and purified by their respective affinity tags. For kinase assays, the SUMO tag was cleaved from IκBα proteins. His–ULD and His–ULD–SDD of hIKKβ were also expressed in *E. coli* using the pET28a vector.

Crystallization and data collection. Unlike many protein kinases, the IKKβ KD cannot be recombinantly expressed as a well-behaved biochemical entity for structural studies. In addition, after mapping a compact region by limited proteolysis, IKKβ was still refractory to crystallization, both alone and in the presence of various ATP analogues. To overcome this obstacle, we used several IKKβ inhibitors, including Cmpd1 and Cmpd2 (Supplementary Fig. 1), which were identified against the S177E/S181E (EE) mutant, in co-crystallization. A hIKKβ EE construct (1–678) lacking only the C-terminal NBD did crystallize; however, these crystals only diffracted to a resolution of ~7.5 Å. Searching IKKβ orthologues that may give better crystals led to success in crystallizing the analogous region of xIKKβ EE (4–675; Fig. 1a).

The xIKKβ (S177E/S181E) protein containing residues 4–675 was concentrated by ultrafiltration (Amicon) to about 15 mg ml^{-1} in 20 mM Tris-HCl (pH 8.0), 150 mM NaCl and 10 mM dithiothreitol (DTT). It was mixed with an inhibitor compound in a 1:2 molar ratio before crystallization. Cmpd1 is 4-((4-(4-(chlorophenyl)pyrimidin-2-yl)amino)phenyl)(4-(2-hydroxyethyl)piperazin-1-yl)methanone and Cmpd2 is 1-(4-(4-((4-(4-(pyridin-4-ylsulfonyl)phenyl)-pyrimidin-2-yl)amino)benzoyl)piperazin-1-yl)ethanone. The *P*1 crystals were grown using hanging-drop vapour diffusion at 4 °C by mixing equal volumes of the purified protein and the crystallization condition of 100 mM *N*-(2-acetamido) iminodiacetic acid at pH 6.5, 10% (w/v) polyethylene glycol 6000, 50 mM Li_2SO_4, 300 mM NaCl and 10 mM DTT. The $I4_122$ crystals were grown at 4 °C with well solution containing 1.8 M K/Na phosphate at pH 5.6 and 10 mM DTT. For data collection, all crystals were flash frozen in the respective crystallization conditions supplemented with 25% (v/v) ethylene glycol. Diffraction data were collected at the 24ID-C beam line of the Advanced Photon Source. Multiwavelength anomalous diffraction (MAD) data on heavy-atom derivative crystals or selenomethionyl crystals were collected near the respective absorption edges. All diffraction data were processed using the HKL2000 suite[43] and their statistics are shown in Supplementary Table 1 and Supplementary Table 2.

Structure determination, refinement and analysis. The initial xIKKβ crystals grew in the *P*1 space group in the presence of the inhibitor Cmpd1 or Cmpd2 and diffracted to a resolution of 3.6 Å. Selenomethionyl crystals were obtained, but we failed to locate the large number of expected selenium sites. Among the extensive heavy-atom searches, an ytterbium-derivative was obtained, with eight well-defined sites, which probably correspond to eight IKKβ molecules in the asymmetric unit. However, the electron density map calculated from a three-wavelength ytterbium-anomalous diffraction data set was insufficient for tracing, and phase combination with the selenomethionyl data set could not be performed, owing to non-isomorphism.

The structure determination was eventually successful in the alternative crystal form, $I4_122$, which contains one molecule of IKKβ in complex with Cmpd1 and diffracted to a resolution of 4.0 Å, using MAD of the selenomethionyl crystals (Supplementary Tables 1 and 2 and Supplementary Fig. 2). Twelve selenium sites were determined using the program SHELXD[44] and refined with the program MLPHARE in the CCP4 suite[45]. MAD phases were calculated at a resolution of 4.0 Å with data from $I4_122$ crystals using the program SHARP[46]. A few cycles of model building and refinement were carried out with the program O[47] and REFMAC with TLS parameterization[48]. The $I4_122$ crystals contain one monomer in the asymmetric unit and 80% solvent when calculated with the entire IKKβ construct and 84% solvent when considering only the ordered part of the structure. The inhibitor Cmpd1 has density in the MAD experimental map and the $F_o - F_c$ omit map. The Dundee PRODRG2 Server was used to generate topology and restraint files of the compound for refinement. The refined model contains residues 16–236, 243–286, 290–376, 384–394, 401–475 and 528–637 and Cmpd1.

The structure of the *P*1 form was determined by molecular replacement using the refined model of the $I4_122$ crystal form as the search model, in which eight molecules were located. Selenium sites of the single-wavelength anomalous diffraction data set of a selenomethionyl crystal in the *P*1 space group was calculated by difference Fourier analysis and used to verify residue registration in the *P*1 structure. Refinement in the *P*1 structure was conducted at a resolution of 3.6 Å and incorporated tight non-crystallographic symmetry restraints (root mean squared deviation of 0.02 Å in atom positions). After several rounds of refinement at a resolution of 3.6 Å, new electron densities appeared in the *P*1 crystal form to complete the model building. Although Cmpd2 was in the crystallization condition, it did not have clear density and was not included in the refinement. The refined model of the *P*1 crystal form contains four IKKβ dimers in the asymmetric unit. Three of the dimers encompass residues 16–236, 243–286, 290–376, 384–394, 401–551 and 559–666. One dimer contains the same residues as the structure in $I4_122$. The structures were analysed using the CCP4 suite[45] and the Dali server[49], and the figures were made using PYMOL[50].

GST pull-down. The tagged proteins were first purified with glutathione or Ni-NTA beads and their expression levels were assessed by SDS–polyacrylamide gel electrophoresis (SDS–PAGE). Beads containing estimated equivalent quantities of the tagged proteins were mixed with the cell lysates or the purified versions of the interaction partners. The mixtures were incubated at room temperature (20 °C) for 1 h with rotation. After centrifugation, the supernatants were removed. The beads were then washed twice, eluted and subjected to SDS–PAGE analysis. All pull-down experiments were repeated two to four times with consistency.

Kinase assays using anti-phospho-IκBα antibody. The hIKKβ proteins (0.1 μg μl^{-1}) were incubated with recombinant IκBα (1 μg μl^{-1}) in 50 mM Tris-HCl at pH 8.0, 100 mM NaCl, 10 mM $MgCl_2$ and 2 mM DTT for 30 min at 30 °C. SDS–PAGE sample buffer was used to terminate the reactions. The products were separated on 15% SDS–PAGE and transferred to PVDF membranes. Anti-phospho-IκBα antibody (Cell Signaling Technology) was used to detect phospho-IκBα.

Determination of K_m of hIKKβ for IκBα (1–54) and full-length IκBα. To derive the K_m of hIKKβ for full-length IκBα, kinase assays were performed at substrate concentrations of 2.8, 5.3, 10.6, 21.3, 42.5 and 85 μM. Similarly, to derive the K_m of hIKKβ for IκBα (1–54), kinase assays were performed at substrate concentrations of 5.3, 10.6, 21.3, 42.5, 85 and 170 μM. A time course of the kinase reactions was first performed to select a hIKKβ amount and a time point within which the reactions are linear with time. The final selected reactions contain 10 ng baculovirus-expressed hIKKβ, 100 mM cold ATP and 1 μl [γ-^{32}P]ATP (3,000 Ci mmol^{-1}, 1 mCi per 100 μl) in 25 μl of reaction buffer containing 50 mM Tris-HCl at pH 8.0, 100 mM NaCl, 10 mM $MgCl_2$ and 2 mM DTT. The phosphotransfer reaction was allowed to proceed for 10 min at 30 °C and quenched with SDS–PAGE sample buffer. The products were separated on 15% SDS–PAGE and subjected to autoradiography. The relative amounts of phosphorylated IκBα were quantified using IMAGEJ, plotted against total IκBα concentrations and fitted using nonlinear regression to the Michaelis–Menten equation to obtain K_m using SIGMAPLOT.

Transfection, immunoprecipitation and kinase assay. The constructs Flag–hIKKβ EE and its truncation mutants; HA–hIKKβ EE and its dimerization mutants L654D/W655D, W655D/L658D and L654D/W655D/L658D; and Flag–hIKKβ and its dimerization mutants L654D/W655D and W655D/L658D were generated in the vector pcDNA3 by conventional PCR. All IKKβ constructs were transfected in HEK293T cells with Lipofectamine 2000 (Invitrogen). After 24 h, cell extracts were immunoprecipitated with anti-Flag antibodies bound to agarose beads (M2, Sigma) or anti-HA bound to agarose beads (Sigma). IKKβ kinase assays were essentially done as previously described[6,13]. Briefly, immunoprecipitates were incubated with 2 μM full-length IκBα (1–317) in 20 mM HEPES at pH 7.5, 10 mM $MgCl_2$, 20 mM β-glycerophosphate, 10 mM PNPP, 50 mM Na_3VO_4, 1 mM DTT, 20 mM ATP, and 1–10-mCi [γ-^{32}P]ATP at 30 °C for 30 min, and subjected to SDS–PAGE and autoradiography. Immunoblotting was performed using anti-Flag (Sigma), anti-HA (Sigma) or anti-IKKβ antibodies (Upstate, 05-535).

Equilibrium analytical ultracentrifugation measurements. Experiments were performed in a Beckman XL-A/I analytical ultracentrifuge (Beckman-Coulter), using six-cell centre pieces with straight walls, a 12-mm path length and sapphire windows. Samples were kept and diluted in 50 mM Tris-HCl at pH 8.0 and 300 mM NaCl. Samples from wild-type protein were diluted to 6.9, 4.5 and 2.4 μM, mutant L654D/W655D to 7.4, 4.8 and 2.6 μM and mutant W655D/L658D to 4.9, 3.2 and 1.7 μM for channels A, B and C, respectively. Dilution buffer was used as blank. All samples were run at 4 °C at 9,000 r.p.m. (5,900*g*; held for 20 h then scanned four times at 1-h intervals), 11,000 r.p.m. (8,800*g*; held for 10 h then scanned four times at 1-h intervals), 14,000 r.p.m. (14,300*g*; held for

10 h then scanned four times at 1-h intervals) and 17,000 r.p.m. (21,000*g*; held for 10 h then scanned four times at 1-h intervals). Detection was by ultraviolet absorption at 280 nm. Solvent density and the protein partial specific volume at each temperature were determined using the program SEDNTERP (Alliance Protein Laboratories). For calculation of K_D and the apparent molecular weight, all useful data were used in a global fit, using the program HETEROANALYSIS, obtained from University of Connecticut (http://www.biotech.uconn.edu/auf).

43. Otwinowski, Z. & Minor, W. Processing of X-ray diffraction data collected in oscillation mode. *Methods Enzymol.* **276,** 307–326 (1997).
44. Schneider, T. R. & Sheldrick, G. M. Substructure solution with SHELXD. *Acta Crystallogr. D* **58,** 1772–1779 (2002).
45. Collaborative Computational Project, Number 4. The *CCP4* suite: programs for protein crystallography. *Acta Crystallogr. D* **50,** 760–763 (1994).
46. Bricogne, G. *et al.* Generation, representation and flow of phase information in structure determination: recent developments in and around SHARP 2.0. *Acta Crystallogr. D* **59,** 2023–2030 (2003).
47. Jones, T. A., Zou, J.-Y., Cowan, S. W. & Kjeldgaard, M. Improved methods for building models in electron density maps and the location of errors in those models. *Acta Crystallogr. A* **47,** 110–119 (1991).
48. Winn, M. D., Murshudov, G. N. & Papiz, M. Z. Macromolecular TLS refinement in REFMAC at moderate resolutions. *Methods Enzymol.* **374,** 300–321 (2003).
49. Holm, L. & Sander, C. Dali: a network tool for protein structure comparison. *Trends Biochem. Sci.* **20,** 478–480 (1995).
50. DeLano, W. L. *PyMOL Molecular Viewer* ⟨http://www.pymol.org⟩ (2002).

Supplementary Table 1. Data collection, phase determination and refinement statistics

	Native 1 (with Cmpd2)	Native 2-Cmpd1	SeMet-Cmpd1		
			Peak	Inflection	High Energy Remote
Data collection	APS 24-ID-C	APS 24-ID-C	APS 24-ID-C	APS 24-ID-C	APS 24-ID-C
Wavelength (Å)	0.97922	0.97922	0.97916	0.97933	0.96394
Space group	P1	$I4_122$	$I4_122$	$I4_122$	$I4_122$
Resolution (Å)	30.0-3.6 (3.66-3.6)	30.0-4.0 (4.07-4.0)	30.0-4.0 (4.07-4.0)	30.0-4.0 (4.07-4.0)	30.0-4.0 (4.07-4.0)
Observations	90,090	15,817	15,861	15,804	15,750
Redundancy	1.9 (1.8)	6.9 (4.7)	12.5 (6.5)	12.4(6.5)	12.1(6.2)
Data coverage (%)	92.5 (76.6)	97.3 (86.3)	98.6 (93.3)	98.1 (90.8)	98.1 (89.0)
I / σ	9.2 (1.5)	25.3 (2.1)	24.7 (1.9)	23.3(1.9)	21.5(1.6)
R_{sym} (%)	7.2 (40.5)	7.8 (36.5)	11.4 (47.3)	11.1 (48.7)	11.4 (50.3)
MAD Analysis					
Resolution (Å)			30-4.0	30-4.0	30-4.0
Phasing power (anomalous)			1.22	1.10	0.94
R_{cullis} (anomalous)			0.87	0.88	0.92
Mean FOM			0.519		
Refinement					
Resolution range (Å)	15.0-3.6	15.0-4.0			
No. reflections	72,261	12,469			
No. atoms	39,106	4,399			
R (%)	30.7	24.9			
R_{free} (%)	34.1	32.4			
Mean B-factors ($Å^2$), overall	192.4	207.9			
Mean B-factors ($Å^2$), Cmpd1		259.9			
R.m.s deviations					
Bonds (Å)	0.058	0.043			
Angles (°)	2.53	2.19			
Ramachandran plot					
Most favored / allowed	79.3% / 96.6%	74.2% / 94.5%			

Highest resolution shell is shown in parenthesis.

Supplementary Table 2. Additional crystallographic statistics

	SeMet	Ytterbium		
Data collection	Peak	Peak	Inflection	Remote
Beam line	APS 24-ID-C	APS 24-ID-C	APS 24-ID-C	APS 24-ID-C
Wavelength (Å)	0.9792	1.3855	1.3860	1.3753
Space group	P1	P1	P1	P1
Cell dimensions a, b, c (Å)	103.4, 140.5, 160.9	97.6, 141.8, 165.8	97.6, 141.8, 165.8	97.6, 141.9, 165.8
α, β, γ (°)	71.4, 79.8, 86.0	69.3, 75.3, 87.9	69.3, 75.3, 87.9	69.3, 75.3, 87.9
Resolution (Å)	30 - 4.3 (4.45 - 4.3)	30 - 4.1 (4.25 - 4.1)	30 - 4.1 (4.25 - 4.1)	30 - 4.1 (4.25 - 4.1)
Observations	55,903	55,456	54,567	55,058
Redundancy	4.5 (4.4)	3.4 (3.0)	3.4 (3.0)	3.3 (3.0)
Data coverage (%)	97.5 (95.4)	88.8 (70.9)	87.5 (68.2)	88.2 (69.3)
I / σ	15.0 (3.5)	11.8 (2.0)	11.3 (1.8)	10.8 (1.6)
R_{sym} (%)	12.2 (49.6)	12.1 (43.3)	12.0 (49.1)	12.3 (55.3)
MAD Analysis				
Resolution (Å)		30 - 4.1	30 - 4.1	30 - 4.1
Phasing power (anomalous)		0.32	0.26	-
R_{cullis} (anomalous)		0.93	0.94	0.98
Mean FOM		0.25		

Highest resolution shell is shown in parenthesis.

Supplementary Table 3. Structural similarity among the 8 independent IKKβ copies in the P1 space group and with IKKβ in the $I4_122$ space group

Reference chain	Alignment chain	R.M.S.D	# Residues aligned
A in P1	B in P1	0.73	480 out of 622
	C in P1	0.62	611 out of 622
	D in P1	0.69	519 out of 622
	E in P1	0.72	582 out of 622
	F in P1	0.72	528 out of 622
	G in P1	0.70	492 out of 541
	H in P1	0.76	528 out of 541
	A in $I4_122$	1.00	472 out of 541

Supplementary Figure 1. Structural formulas of the IKKβ inhibitors Cmpd1 and Cmpd2. The piperazine ring, the first phenyl ring, the pyrimidine ring and the second phenyl ring are labeled with A, B, C and D, respectively.

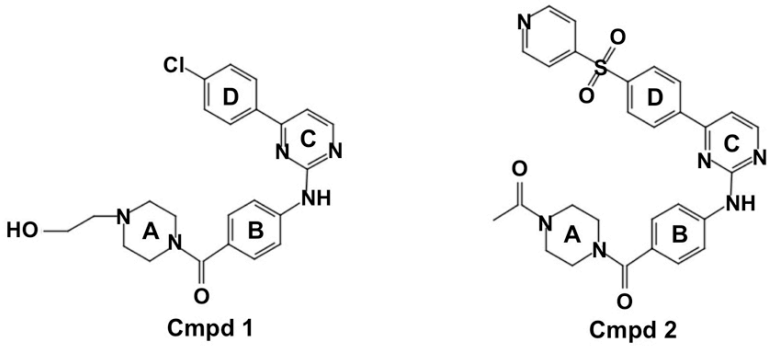

Supplementary Figure 2. MAD experimental electron density map in the $I4_122$ space group (left) and 2Fo-Fc map in the P1 space group (right), contoured at 1.5 σ (cyan) and superimposed with the trace of the final model (yellow)

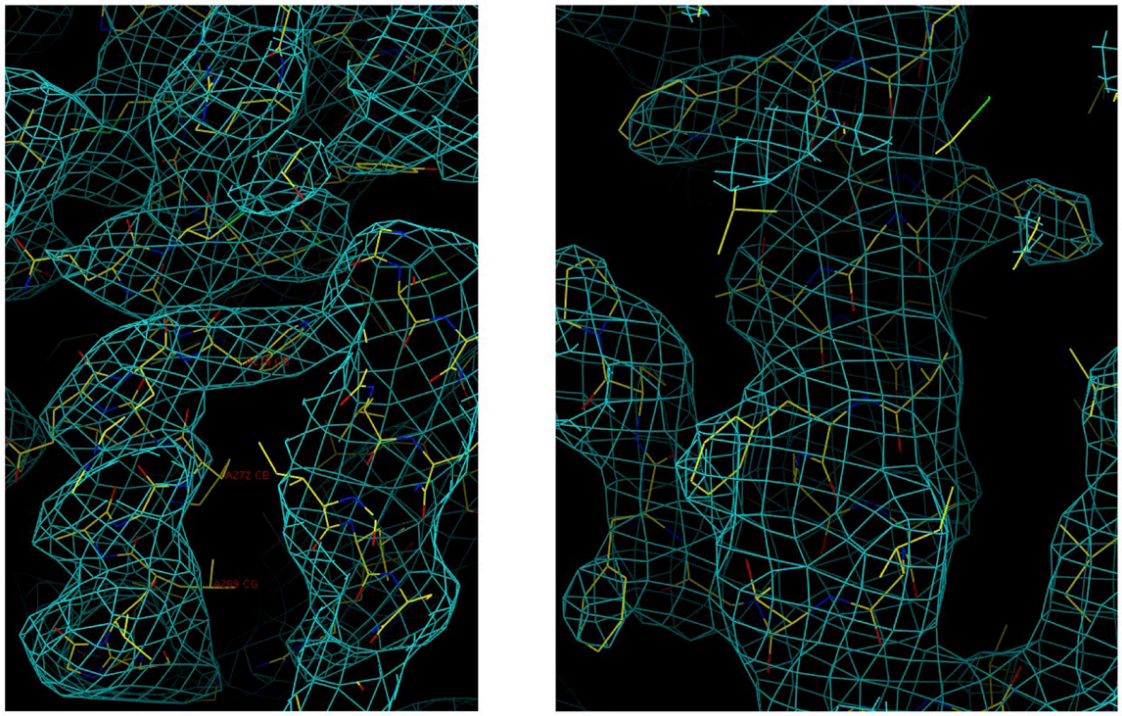

MAD map of $I4_122$ | 2Fo-Fc map of P1

Supplementary Figure 3. Superposition among the 8 independent copies of xIKKβ in the P1 structure (a) and between one copy of xIKKβ in the P1 structure (green) and the $I4_122$ structure (black) (b).

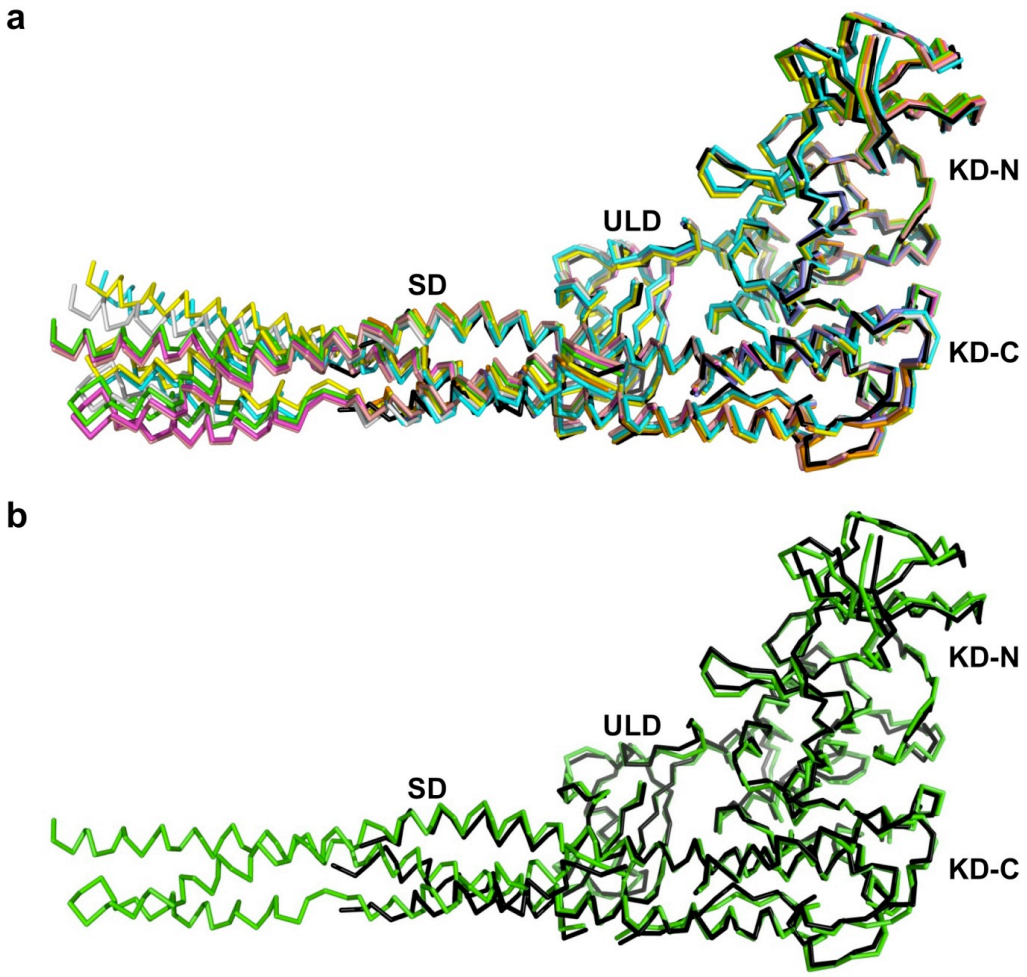

Supplementary Figure 4. Sequence alignment of IKKβ orthologues, human IKKα and mouse PKA. hIKKβ: human IKKβ; mIKKβ: mouse IKKβ; oIKKβ: opossum IKKβ; xIKKβ: Xenopus laevis IKKβ; cIKKβ: chicken IKKβ; hIKKα: human IKKα; mPKA: mouse PKA. Conserved residues are highlighted in yellow. β-stands are indicated with arrows and α-helices are shown in cylinders, with orange for KD-N, yellow for KD-C, magenta for ULD and blue for SDD. The two MAPKK consensus activation loop Ser residues S177 and S181 are indicated by red dots above the alignment. Conserved catalytic residues are indicated with black triangles. Residues on the KD-SDD interface, the ULD-SDD interface, and the ULD-KD interface are indicated with orange diamonds, blue dots and green crosses, respectively. Residues at the dimerization interface are shown as red arrows. Buried residues in the ULD domain are indicated with magenta dots on the bottom.

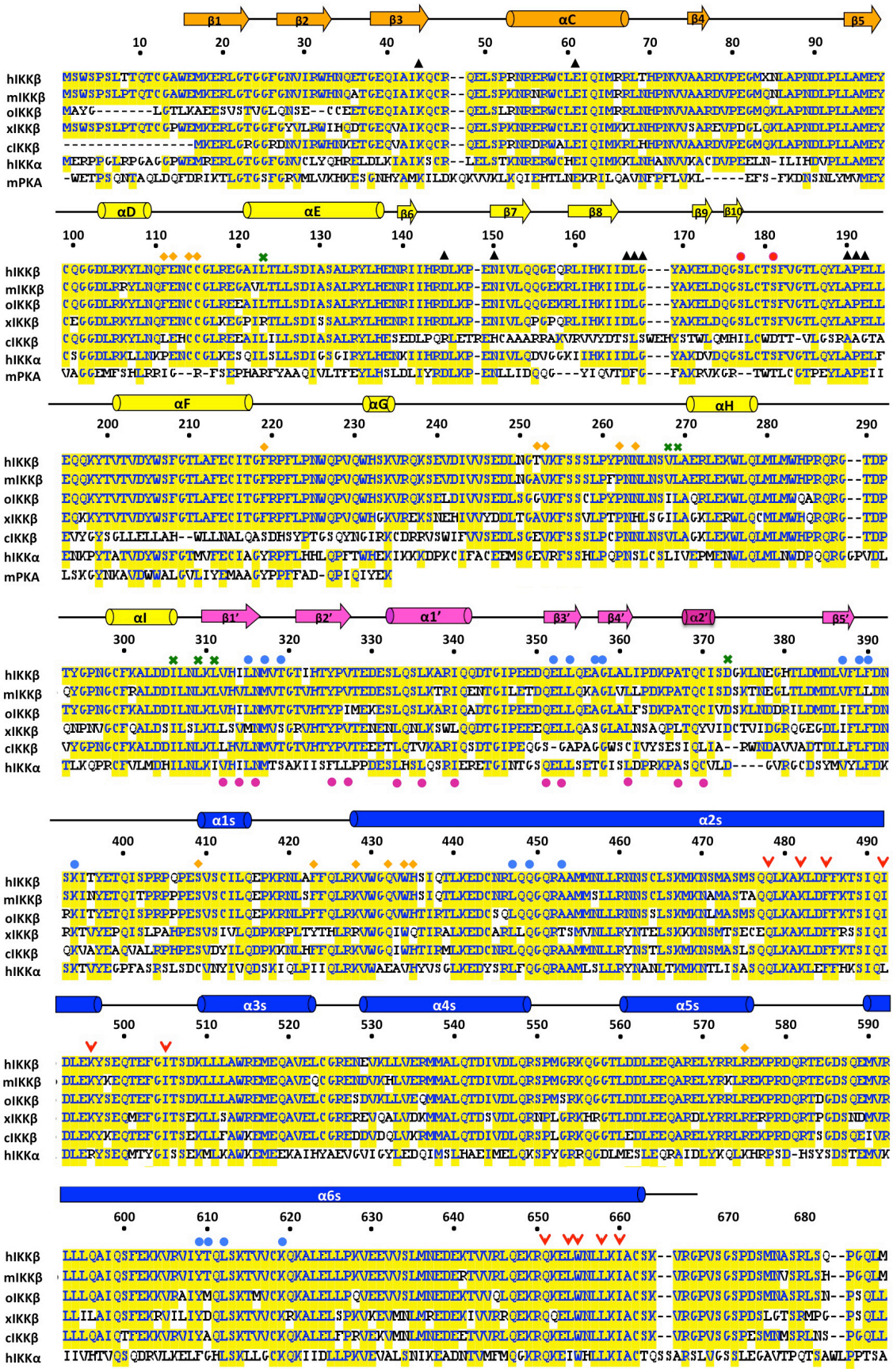
β1 β2 β3 αC β4 β5
hIKKβ MSWSPSLTTQTCGAWEMKERLGTGGFGNVIRWHNQETGEQIAIKQCR--QELSPRNRERWCLEIQIMRRLTHPNVVAARDVPEGMQNLAPNDLPLLAMEY
mIKKβ MSWSPSLPTQTCGAWEMKERLGTGGFGNVIRWHNQATGEQIAIKQCR--QELSPKNRNRWCLEIQIMRRLNHPNVVAARDVPEGMQNLAPNDLPLLAMEY
oIKKβ MAYG-------LGTLKAEESVSTVGLQNSE--CCEETGEQIAIKQCR--QELSLRNRERWCLEIQIMRRLNHPNVVAARDVPEGMQKLAPNDLPLLAMEY
xIKKβ MSWSPSLPTQTCGPWEMKERLGTGGFGYVLRWIHQDTGEQVAIKQCR--QELSPKNRERWCLEIQIMKKLNHPNVVSAREVPDGLQKLAPNDLPLLAMEY
cIKKβ ----------------MKERLGRGGRDNVIRWHNKETGEQVAIKQCR--QELSPRNRDRWALEIQIMKRLNHPNVVAARDVPEGMQKLAPNDLPLLAMEY
hIKKα MERPPGLRPGAGGPWEMERERLGTGGFGNVCLYQHRELDLKIAIKSCR--LELSTKNRERWCHEIQIMKKLNHANVVKACDVPEELN-ILIHDVPLLAMEY
mPKA -WETPSQNTAQLDQFDRIKTLGTGSFGRVMLVKHKESGNHYAMKILDKQKVVKLKQIEHTLNEKRILQAVNFPFLVKL-----EFS-FKDNSNLYMVMEY
αD αE β6 β7 β8 β9 β10
hIKKβ CQGGDLRKYLNQFENCCGLREGAILTLLSDIASALRYLHENRIIHRDLKP-ENIVLQQGEQRLIHKIIDLG---YAKELDQGSLCTSFVGTLQYLAPELL
mIKKβ CQGGDLRRYLNQFENCCGLREGAVLTLLSDIASALRYLHENRIIHRDLKP-ENIVLQQGEKRLIHKIIDLG---YAKELDQGSLCTSFVGTLQYLAPELL
oIKKβ CQGGDLRKYLNQFENCCGLREEAILTLLSDIASALRYLHENRIIHRDLKP-ENIVLQQGEKRLIHKIIDLG---YAKELDQGSLCTSFVGTLQYLAPELL
xIKKβ CEGGDLRKYLNQFENCCGLKEGPIRTLLSDISSALRYLHENRIIHRDLKP-ENIVLQPGPQRLIHKIIDLG---YAKELDQGSLCTSFVGTLQYLAPELL
cIKKβ CQGGDLRKYLNQLEHCCGLREEAILILLSDIASALRYLHESEDLPQRLETREHCAAARRAKVRVVYDTSLSWEHYSTWLQMHILCWDTT-VLGSRAAGTA
hIKKα CSGGDLRKLLNKPENCCGLKESQILSLLSDIGSGIRYLHENKIIHRDLKP-ENIVLQDVGGKIIHKIIDLG---YAKDVDQGSLCTSFVGTLQYLAPELF
mPKA VAGGEMFSHLRRIG--R-FSEPHARFYAAQIVLTFEYLHSLDLIYRDLKP-ENLLIDQQG---YIQVTDFG---FAKRVKGR--TWTLCGTPEYLAPEII
αF αG αH
hIKKβ EQQKYTVTVDYWSFGTLAFECITGFRPFLPNWQPVQWHSKVRQKSEVDIVVSEDLNGTVKFSSSLPYPNNLNSVLAERLEKWLQLMLMWHPRQRG--TDP
mIKKβ EQQKYTVTVDYWSFGTLAFECITGFRPFLPNWQPVQWHSKVRQKSEVDIVVSEDLNGAVKFSSSLPFPNNLNSVLAERLEKWLQLMLMWHPRQRG--TDP
oIKKβ EQQKYTVTVDYWSFGTLAFECITGFRPFLPNWQPVQWHSKVRQKSELDIVVSEDLSGGVKFSSCLPYPNNLNSILAQRLEKWLQLMLMWQARQRG--TDP
xIKKβ EQKKYTVTVDYWSFGTLAFECITGFRPFLPNWQPVQWHGKVREKSNEHIVVYDDLTGAVKFSSVLPTPNHLSGILAGKLERWLQCMLMWHQRQRG--TDP
cIKKβ EVYGYSGLLELLAH--WLLNALQASDHSYPTGSQYNGIRKCDRRVSWIFVVSEDLSGEVKFSSSLPCPNNLNSVLAGKLEKWLQLMLMWHPRQRG--TDP
hIKKα ENKPYTATVDYWSFGTMVFECIAGYRPFLHHLQPFTWHEKIKKKDPKCIFACEEMSGEVRFSSHLPQPNSLCSLIVEPMENWLQLMLNWDPQQRGGPVDL
mPKA LSKGYNKAVDWWALGVLIYEMAAGYPPFFADQPIQIYEK
αI β1′ β2′ α1′ β3′ β4′ α2′ β5′
hIKKβ TYGPNGCFKALDDILNLKLVHILNMVTGTIHTYPVTEDESLQSLKARIQQDTGIPEEDQELLQEAGLALIPDKPATQCISDGKLNEGHTLDMDLVFLFDN
mIKKβ QYGPNGCFRALDDILNLKLVHVLNMVTGTVHTYPVTEDESLQSLKTRIQENTGILETDQELLQKAGLVLLPDKPATQCISDSKTNEGLTLDMDLVFLLDN
oIKKβ TYGPNGCFKALDDILNLKLVHILNMVTGTVHTYPIMEKESLQSLKARIQADTGIPEEDQELLQEAGLALFSDKPATQCIVDSKLNDDPILDMDLIFLFDN
xIKKβ QNPNVGCFQALDSILSLKLLSVMNMVSGRVHTYPVTENENLQNLKSWLQQDTGIPEEEQELLQASGLALNSAQPLTQYVIDCTVIDGRQGEGDLIFLFDN
cIKKβ VYGPNGCFKALDDILNLKLLHVLNMVTGTVHTYPVTEEETLQTVKARIQSDTGIPEQGS-GAPAGGWSCIVYSESIQLIA--RWNDAVVADTDLLFLFDN
hIKKα TLKQPRCFVLMDHILNLKIVHILNMTSAKIISFLLPPDESLHSLQSRIERETGINTGSQELLSETGISLDPRKPASQCVLD----GVPGCDSYMVYLFDK
α1s α2s
hIKKβ SKITYETQISPRPQPESVSCILQEPKRNLAFFQLRKVWGQVWHSIQTLKEDCNRLQQGQRAAMMNLLRNNSCLSKMKNSMASMSQQLKAKLDFFKTSIQI
mIKKβ SKINYETQITPRPPPESVSCILQEPKRNLSFFQLRKVWGQVWHSIQTLKEDCNRLQQGQRAAMMSLLRNNSCLSKMKNAMASTAQQLKAKLDFFKTSIQI
oIKKβ RKITYETQISPRPPPESVSCILQEPKRNLPFFQLRKVWGQVWHTIRTLKEDCSQLQQGQRAAMMNLLRNNSSLSKMKNLMASMSQQLKAKLDFFKTSIQI
xIKKβ RKTVYEPQISLPAHPESVSIVLQDPKRPLTYTHLRRVWGQIWQTIRALKEDCARLLQGQRTSMVNLLRYNTELSKKKNSMTSECEQLKAKLDFFRSSIQI
cIKKβ QKVAYEAQVALRPHPESVDYILQDPKKNLHFTQLRKVWGQIWHTIRMLKEDCNRLQQGQRAAMMNLLRYNSTLSKMKNSMASLSQQLKAKLDFFKTSIQI
hIKKα SKTVYEGPFASRSLSDCVNYIVQDSKIQLPIIQLRKVWAEAVHYVSGLKEDYSRLFQGQRAAMLSLLRYNANLTKMKNTLISASQQLKAKLEFFHKSIQL
α3s α4s α5s
hIKKβ DLEKYSEQTEFGITSDKLLLAWREMEQAVELCGRENEVKLLVERMMALQTDIVDLQRSPMGRKQGGTLDDLEEQARELYRRLREKPRDQRTEGDSQEMVR
mIKKβ DLEKYKEQTEFGITSDKLLLAWREMEQAVEQCGRENDVKHLVERMMALQTDIVDLQRSPMGRKQGGTLDDLEEQARELYRKLREKPRDQRTEGDSQEMVR
oIKKβ DLEKYSEQTEFGITSDKLLLAWREMEQAVELCGRESDVKLLVEQMMALQTDIVDLQRSPMSRKQGGTLDDLEEQARELYRRLREKPRDQRTDGDSQEMVR
xIKKβ DLEKYSEQMEFGITSEKLLSAWREMEQAVELCGREREVQALVDKMMALQTDSVDLQRNPLGRKHRGTLDDLEEQARDLYRRLREKPRDQRTPGDSNDMVR
cIKKβ DLEKYKEQTEFGITSEKLLFAWKEMEQAVELCGREDDVDQLVKRMMALQTDIVDLQRSPLGRKQGGTLEDLEEQAPELYRRLREKPRDQRTSGDSQEIVR
hIKKα DLERYSEQMTYGISSEKMLKAWKEMEEKAIHYAEVGVIGYLEDQIMSLHAEIMELQKSPYGRRQGDLMESLEQRAIDLYKQLKHRPSD-HSYSDSTEMVK
α6s
hIKKβ LLLQAIQSFEKKVRVIYTQLSKTVVCKQKALELLPKVEEVVSLMNEDEKTVVRLQEKRQKELWNLLKIACSK--VRGPVSGSPDSMNASRLSQ--PGQLM
mIKKβ LLLQAIQSFEKKVRVIYTQLSKTVVCKQKALELLPKVEEVVSLMNEDERTVVRLQEKRQKELWNLLKIACSK--VRGPVSGSPDSMNVSRLSH--PGQLM
oIKKβ LLLQAIQSFEKKVRAIYMQLSKTMVCKQKALELLPQVEEVVSLMNEDEKTVVQLQEKRQKELWNLLKIACSK--VRGPVSGSPDSMNASRLSN--PSQLL
xIKKβ LLILAIQSFEKRVILIYDQLSKTVVCKRKALELSPKVKEVMNLMREDEKIVVRRQEKRQQELWNLLKIACSK--VRGPVSGSPDSLGTSPMPG--PSQLL
cIKKβ LLLQAIQTFEKKVRVIYAQLSKTVVCKQKALELFPRVEKVMNLMNEDEETVVRLQEKRQKELWNLLKIACSK--VRGPVSGSPESMNMSRLNS--PGQLL
hIKKα IIVHTVQSQDRVLKELFGHLSKLLGCKQKIIDLLPKVEVALSNIKEADNTVMFMQGKRQKEIWHLLKIACTQSSARSLVGSSLEGAVTPQTSAWLPPTSA

Supplementary Figure 5. Alignment between ULD and Ub, showing the three conserved hydrophobic residues and residues at the interface with SDD

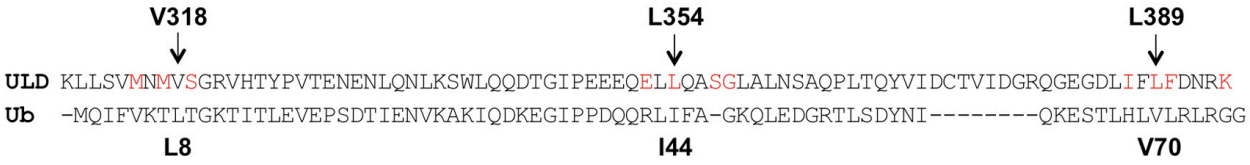

Supplementary Figure 6. MAD map at 1.0 σ in the $I4_122$ space group

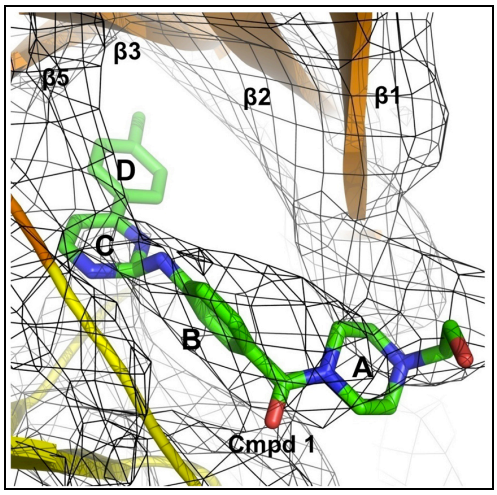

Supplementary Figure 7. Superposition among the 4 non-crystallographic xIKKβ dimers in the P1 space group and the 1 crystallographic xIKKβ dimer in the $I4_122$ space group

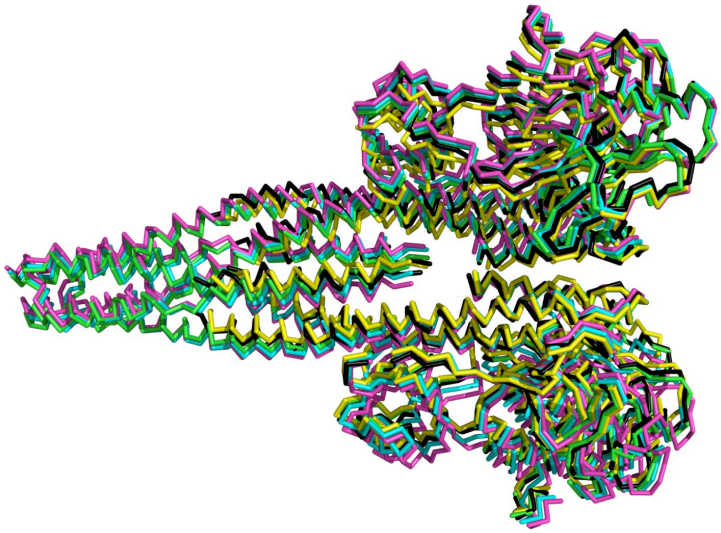

Supplementary Figure 8. SDS-PAGE of washed xIKKβ crystals in the $I4_122$ space group

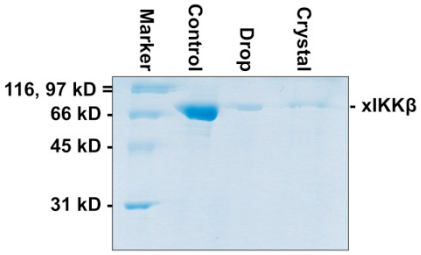

Supplementary Figure 9. A model of the full IKK complex dimer showing the possibly extremely elongated nature of the complex

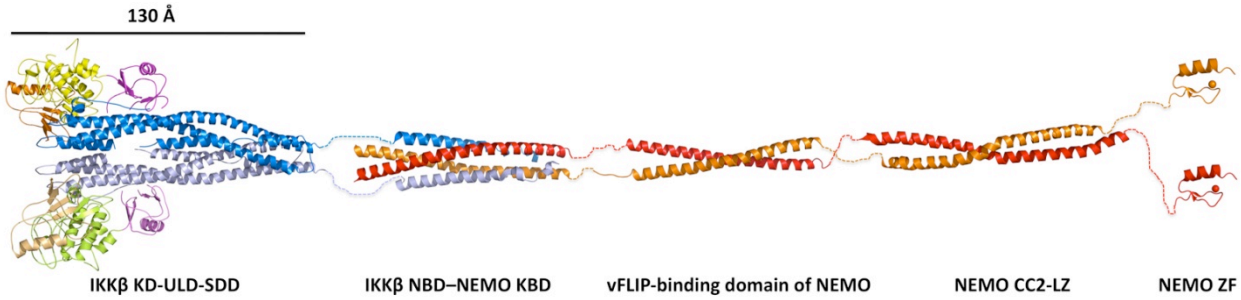

Supplementary Figure 10. Superposition of the 2 non-crystallographic xIKKβ tetramers in the P1 space group and the 1 crystallographic xIKKβ tetramer in the $I4_122$ space group